ACS OMEGA

http://pubs.acs.org/journal/acsodf

Article

Noncatalytic Oxidative Coupling of Methane (OCM): Gas-Phase Reactions in a Jet Stirred Reactor (JSR)

Haoyi Wang,* Can Shao, Jorge Gascon, Kazuhiro Takanabe, and S. Mani Sarathy*

Cite This: *ACS Omega* 2021, 6, 33757−33768

Read Online

ACCESS | Metrics & More | Article Recommendations | Supporting Information

ABSTRACT: Oxidative coupling of methane (OCM) is a promising technique for converting methane to higher hydrocarbons in a single reactor. Catalytic OCM is known to proceed via both gas-phase and surface chemical reactions. It is essential to first implement an accurate gas-phase model and then to further develop comprehensive homogeneous−heterogeneous OCM reaction networks. In this work, OCM gas-phase kinetics using a jet-stirred reactor are studied in the absence of a catalyst and simulated using a 0-D reactor model. Experiments were conducted in OCM-relevant operating conditions under various temperatures, residence times, and inlet CH_4/O_2 ratios. Simulations of different gas-phase models related to methane oxidation were implemented and compared against the experimental data. Quantities of interest (QoI) and rate of production analyses on hydrocarbon products were also performed to evaluate the models. The gas-phase models taken from catalytic reaction networks could not adequately describe the experimental gas-phase performances. NUIGMech1.1 was selected as the most comprehensive model to describe the OCM gas-phase kinetics; it is recommended for further use as the gas-phase model for constructing homogeneous−heterogeneous reaction networks.

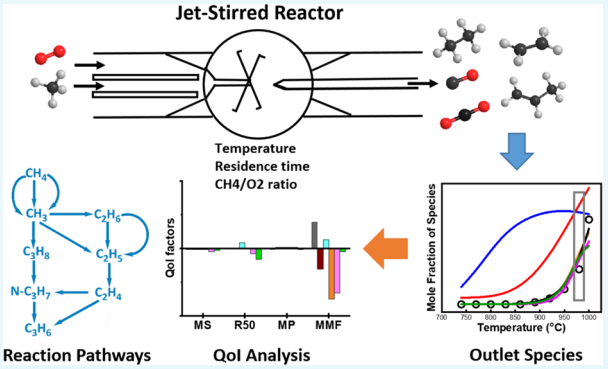

INTRODUCTION

Due to increasingly strict regulations on carbon emissions, production of natural gas (mainly CH_4) has increased dramatically over the past decade and is expected to continue to expand in the foreseeable future. Because of its relatively low economic value, natural gas is attracting worldwide attention by utilizing CH_4 in more valuable chemicals, rather than as an energy source. The oxidative coupling of methane (OCM) is considered to be one of the important routes for directly converting methane into more desirable and valuable higher hydrocarbons, such as olefins, in the presence of catalysts. This process was first introduced by Keller and Bhasin in the 1980s[1] and it has been exhaustively studied over the years to explore suitable catalysts and to find fundamental kinetic studies for commercialization. Other than traditional thermocatalysis, the OCM process has also been developed at ambient temperatures with the application of visible light and electric fields.[2,3] Recently, Siluria Technologies developed several patented technologies and constructed pilot plant units, upgrading the scale for OCM commercialization.[4,5] The OCM process has not yet been fully commercialized and still requires better understanding of both reaction kinetics and catalytic performances on a targeted single pass yield for C_2 products.[6]

The generally accepted OCM pathways consist of both gas-phase (homogeneous) and surface-catalyzed (heterogeneous) reaction networks.[6−11] Oxygen is first adsorbed and dissociated into surface-active oxygen species (O*) in the presence of a catalyst surface (eq 1). One methyl radical then forms via the hydrogen abstraction between CH_4 and O*, whereas two methyl radicals combine in the gas phase to form ethane (eqs 2 and 3). The secondary reaction product ethylene is then formed via dehydrogenation of ethane in both the gas-phase and surface reactions.

$$O_2 + 2^* \leftrightarrow 2O^* \quad (1)$$

$$CH_4 + O^* \rightarrow CH_3\cdot + OH^* \quad (2)$$

$$2CH_3\cdot \rightarrow C_2H_6 \quad (3)$$

The effect of adding water vapor over OCM has been reported to depend on the composition of the catalyst.[10] For example, $Mn/Na_2WO_4/SiO_2$ shows the promotional effect of water vapor at high reaction temperatures above 800 °C,[8,12] whereas water vapor deactivates Li/MgO by gradually removing lithium.[13] From the analysis of reaction pathways of $Mn/Na_2WO_4/SiO_2$, the OH-mediated reaction pathways are favored for higher yields than surface-mediated path-

Received: September 10, 2021
Accepted: November 15, 2021
Published: November 30, 2021

Table 1. General Information of Selected Gas-Phase Models

name	year	ref	# of species	# of reactions	notes
1. AramcoMech3.0	2018	59	579	3037	developed based on AramcoMech 1.3 & 2.0[60,66]
2. CRECK (C_0–C_3)	2020	61	114	1941	developed upon AramcoMech2.0[60] and further modified with experimental data
3. GRI-Mech 3.0	1999	62	53	325	successor of GRI-Mech 2.11
4. Karakaya model	2018	31	23	39	adapted from Sun *et al.*[26] and modified based on experimental data
5. NUIGMech1.1	2020	63	2746	11,270	developed based on experimental and theoretical studies[70−73]
6. Quiceno model	2003	64	29	78	adapted and reduced from the Karbach model[69] for CPO
7. Schwarz model	2014	55	49	328	reduced model of Dooley *et al.*[68] (derived from AramcoMech1.3[66])
8. Sun model	2008	26	23	39	reduced and modified from the experimental study of Chen *et al.*[19]
9. USC Mech II	2007	65	111	784	developed based GRI-Mech 3.0[62] and other experimental studies[74−76]

ways.[8,12] Hydroxyl radicals (OH·) are believed to be generated from water vapor and oxygen in the gas phase, with the presence of a catalyst surface, and abstract hydrogen from methane for initiation (eqs 4 and 5). To support this theory, the formation of hydroxyl radicals has been directly observed using LIF spectroscopy[14] and the contribution of the hydroxyl radical generation rate in the gas-phase network on OCM has also been investigated for simulation study, which could theoretically reach the maximum C_2H_4 yield of 32%.[15]

$$O_2 + 2H_2O \leftrightarrow 4OH\cdot \quad (4)$$

$$CH_4 + OH\cdot \rightarrow CH_3\cdot + H_2O \quad (5)$$

Several homogeneous−heterogeneous OCM mechanisms have been developed based on experimental results with different catalysts to better understand the kinetics of the OCM process and to further screen the maximum achievable C_2 yield with optimum operating conditions. In early studies, a homogeneous−heterogeneous OCM model for Li/MgO was established by Shi *et al.* with 156 gas-phase and 4 surface reactions in which the gas-phase mechanism agreed with the results from the partial oxidation (CPO) of methane.[16] A mechanism was also developed by Mims *et al.* over a Li/MgO catalyst with 447 gas-phase and 4 surface reactions by performing detailed isotopic analysis.[17] On the other hand, the role of the catalysts was reported to be both a producer and quencher for radicals. Couwenberg *et al.*[18] implemented a model with 39 gas-phase chain reactions, coupled with 10 catalytic reactions, to describe the Li/MgO-based catalysts, in which gas-phase chain reactions were adapted and reduced from a homogeneous gas-phase model of OCM by Chen *et al.*[19] Based on these 39 gas-phase reactions, several catalytic mechanisms were further developed over different types of catalysts to describe the catalytic behaviors by their properties, connect the performances with catalytic descriptors among different catalysts, and screen for the optimum catalysts.[20−31] On the other hand, for OCM gas-phase studies, several early studies were investigated by proposing homogeneous models without the presence of a catalyst.[19,32−34] One of the reduced models,[18] as previously mentioned, is selected for further comparison. Luo *et al.*[35] analyzed the gas-phase reaction network over the Li/MgO catalyst with the detection of gas-phase intermediate species. Ishioka *et al.*[36] also used a machine learning technique to better understand the gas-phase performances against operating conditions from the high-throughput experimental data. In fact, since surface species are difficult to observe or identify, OCM surface kinetics are indirectly investigated experimentally by extrapolating conversion rates and selectivity at zero methane conversion for initiation steps[8,12,37−39] or by applying isotopic techniques to identify the pathways of products.[8,17,40−42] Other than these, the parameters of surface elementary reactions (sticking coefficient and activation energy) are estimated mostly via density functional theory (DFT) calculations[43−54] or Polanyi relationships.[20,21,23,25,26] It is challenging to precisely predict the entire surface reaction mechanism for OCM, which indicates the critical role of an accurate and reliable gas-phase model over the entire mechanism. To fulfill this requirement, gas-phase reaction models should accurately describe well-known homogeneous processes (oxidation, pyrolysis, etc.), either with or without the presence of a catalyst surface. In other words, the heterogeneous mechanism should be developed based on accurate gas-phase reaction models, but not *vice versa*.

For reactor selection in this study, plug flow reactors (PFRs) are commonly used for experiments on methane oxidation to generate the homogeneous gas-phase model for OCM.[10,19,26,32,34,35,55] For simulation, they are usually assumed to behave as ideal plug flow reactors (1-D). However, the fluid flow pattern within the reactor (early mixing, radical velocity profiles) can cause variations in the flow regimes, and the transport properties for each species must be well known to accurately define the reaction zone and describe the process.[56] Also, temperature gradients along the reactor could reach up to several hundred degrees with the exothermic process, complicating the simulation and affecting the model's accuracy in the experimental results. In this study, a jet-stirred reactor (JSR) was selected to study the OCM gas-phase kinetics; it could be assumed to provide homogeneous gas compositions with perfect mixing by carefully selecting the reactor dimensions and operating conditions.[57] A steady state was achieved quickly within the reactor, so it was easy to be modeled as a 0-D reactor.[58] Regarding the exothermicity in methane oxidation, the reactant was highly diluted by inert gas to reduce the existence of the temperature gradient within the reactor in order to describe the process more accurately.

In this work, a gas-phase kinetic study of OCM was performed using a jet-stirred reactor, which could be modeled as a 0-D reactor with ideal mixing. The reactor was tested under various operating conditions, including temperatures, residence times, and inlet CH_4/O_2 ratios. Various experimentally validated gas-phase models were also applied under OCM conditions from either strictly gas-phase kinetic studies or from heterogeneous catalysis. Simulations were utilized, given the experimental boundary conditions, and employed to identify the influence of various operating conditions. Quantities of interest (QoI) and rate of production (ROP) analyses on hydrocarbon products were also investigated to identify main reaction pathways and to differentiate among the models. The formation of C_3H_6, a minor but important species

https://doi.org/10.1021/acsomega.1c05020
ACS Omega 2021, 6, 33757−33768

for OCM, was also discussed. The simulation results of selected models were compared against the experimental data and the best model was determined. The main objectives of this work were to examine different gas-phase kinetic models with a 0-D reactor, under methane-rich operating conditions, and to show the essential role of an accurate gas-phase model for developing homogeneous−heterogeneous OCM reaction networks.

RESULTS AND DISCUSSION

Discussion of Selected Models. Nine models, including AramcoMech3.0,[59,60] the CRECK model (C_0−C_3),[61] GRI-Mech 3.0,[62] the Karakaya model,[31] NUIGMech1.1,[63] the Quiceno model,[64] the Schwarz model,[55] the Sun model,[26] and USC Mech II,[65] were chosen in this study for gas-phase simulation under OCM conditions, where all the models were reported with experimental validations for either strictly gas-phase kinetic studies or heterogeneous catalysis for methane oxidation in fuel-rich conditions (CPO or OCM). General information of all the models is listed in Table 1. All the reaction mechanisms had rates expressed in the form of Arrhenius parameters, as shown in eq 6, where A is the pre-exponential factor, and E_a is the activation energy.

$$k = AT^n \exp\left(-\frac{E_a}{RT}\right) \quad (6)$$

Of the chosen models, AramcoMech3.0 was built upon AramcoMech2.0[60] and AramcoMech1.3[66] and accurately described the gas-phase kinetics and thermochemical properties of C_0−C_4. The model was validated against experimental measurements on hydrocarbon oxidation and pyrolysis (C_1−C_4-based hydrocarbon and oxygenated fuels). On the other hand, the newly published mechanism NUIGMech1.1[63] was developed based on experimental and theoretical studies by the National University of Ireland Galway (NUIG), the same team for AramcoMech development. The mechanism was also validated against oxidation of C_1−C_4 hydrocarbons and their mixtures. The CRECK model used in this study[61] was also developed based on AramcoMech2.0[67] and further updated based on experimental validation under MILD and OXY fuel combustion conditions. GRI-Mech 3.0[62] targeted modeling of the combustion of natural gas. USC Mech II[65] was developed based on different combustion models, including GRI-Mech 3.0. It was also validated against the combustion data of C_0−C_4. The model of Schwarz *et al.*[55] was adapted and reduced from Dooley's model,[68] which described the oxidation of methyl formate, and compared it against the experimental data of fuel-rich methane oxidation (OCM condition) in a plug flow reactor. In addition to these four models, from strictly gas-phase studies, as discussed above, two other models were selected from homogeneous−heterogeneous networks for methane oxidation in the presence of catalysts. In this study, only the homogeneous models accounted for gas-phase simulation. The model of Karakaya *et al.*[31] validated the experimental data for OCM over $Mn/Na_2WO_4/SiO_2$ against wide temperature ranges and CH_4/O_2 ratios in a 1-D adiabatic packed bed reactor; its gas-phase model, taken from Sun *et al.*,[26] consisted of 39 elementary reactions with 22 gas-phase species with parameter modifications. The model of Sun *et al.*[26] consists of homogeneous−heterogeneous reaction networks, which were validated against OCM experimental results with Li/MgO and Sn/Li/MgO. The gas-phase part was reduced and modified from the model of Chen *et al.*[19] The model of Quiceno *et al.*[64] captured the trends of partial oxidation of methane (CPO) over Pt gauze and predicted the production of ethane and ethylene from OCM in 3-D flow fields. The homogeneous part of this model was adapted and reduced from the model of total oxidation of C_1−C_4 alkanes at high temperatures.[69]

Effect of Temperature. The input parameters for JSR, as well as inlet compositions, temperatures, and calculated residence times used for simulation, are shown in Table 2,

Table 2. Operating Conditions as Model Input Parameters

parameter input	
nozzle type	crossed nozzles
operating temperature, T	700−1000 °C
reactor volume	76 cm^3
inlet CH_4/O_2 molar ratio	2−6
pressure, P	101 kPa
inlet methane concentration	1−5%, diluted with N_2
residence time (RT), τ	1000−3000 ms
reactor type	perfectly stirred reactor (0-D)

which corresponded to the experimental setup and operating conditions. The temperature effect of gas-phase OCM was studied from 700 to 1000 °C, and the outlet concentration of each main species, including CH_4, C_2H_6, C_2H_4, CO, CO_2, and O_2, is measured and plotted against the measured temperature in Figure 1. Simulation results for each model were compared with experimental data. According to the experimental results, methane conversion was initially observed at approximately 860 °C, which corresponded with the results from the previous literature for a low inlet methane concentration in an oxygen-rich condition.[77] From the observations, C_2H_6 was produced first at lower temperatures under methane-rich operating conditions than CO. From the trends, the product concentrations all increased with the temperature. For reactant consumption (CH_4 and O_2), by comparing experimental data against the simulation results in Figure 1a,f, USC Mech II, GRI-Mech 3.0, CRECK, NUIGMech1.1, and AramcoMech3.0 successfully followed the trend of reactant consumptions and accurately predicted the concentration profiles against temperature. The Schwarz model also captured the general trend of reactant consumption but slightly overestimated the consumption rate at higher temperatures. For product formation, the simulation results of these four models were also in agreement regarding the measured concentration profiles. In Figure 1b, USC Mech II, GRI-Mech 3.0, CRECK, NUIGMech1.1, and the Schwarz model all captured the local concentration plateau of C_2H_6 at 980 °C, while AramcoMech3.0 responded somewhat slower. The Schwarz model overestimated CO production in Figure 1d. The CRECK model overestimated CO_2 production, whereas USC Mech II underestimated it in Figure 1e.

Among the gas-phase models taken from homogeneous−heterogeneous reaction networks, the Sun model did not show any reactivity under all operating conditions in Table 2. Therefore, the simulation results are not plotted for comparison with the experimental data. On the other hand, the Karakaya and Quiceno models significantly overestimated the consumption of reactants: Methane and oxygen were heavily consumed at 740 °C and oxygen was fully consumed at 1000 °C. Because of the overestimated reactant consumptions,

https://doi.org/10.1021/acsomega.1c05020
ACS Omega 2021, 6, 33757−33768

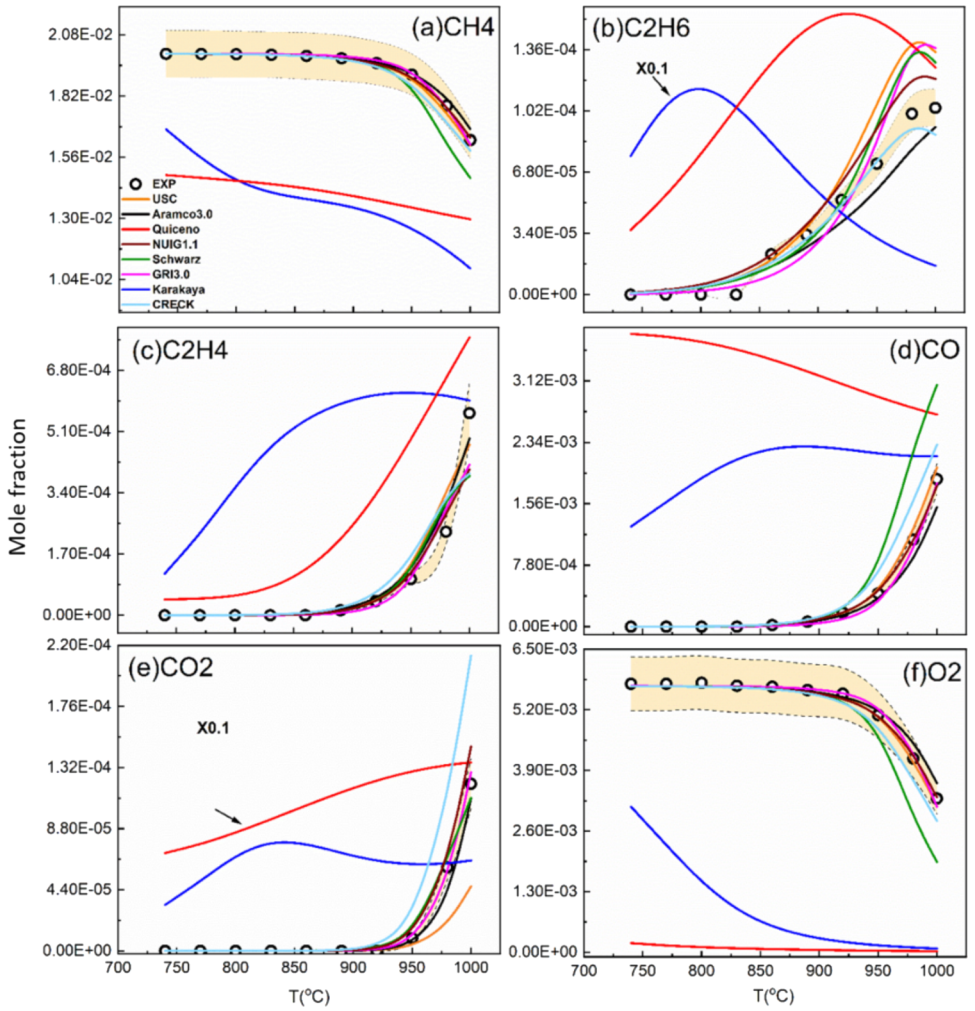

Figure 1. Comparison of mole fraction between experimental (hollow circles) and simulated results (lines with corresponding colors) of (a) CH_4, (b) C_2H_6, (c) C_2H_4, (d) CO, (e) CO_2, and (f) O_2 in the outlet stream against temperature. Operating condition: 2% inlet CH_4, CH_4/O_2 = 3.5, 101 kPa total pressure, N_2 as balance, and RT = 2000 ms. Yellow shadowed regions with dotted lines are error bars for experimental data.

the simulations of each model also displayed completely different trends than the experimental results. Overestimations in concentration for each product can be observed in Figure 1. In Figure 1b, the concentration plateau shifted from 980 °C to 800 °C and 920 °C for the Karakaya and Quiceno models, respectively; for this reason, details of these two models were reviewed to clarify their kinetic pathways. It was found that the gas-phase reactions contributed significantly to the overall homogeneous−heterogeneous network. The homogeneous−heterogeneous model from Karakaya *et al.*[31] predicted significant amounts of gas-phase species for OCM at temperatures ranging from 600 to 850 °C, with inlet CH_4/O_2 ratios of 2, 5, and 10, respectively, even in the absence of a catalyst bed. On the other hand, Quiceno *et al.*[64] studied the catalytic partial oxidation (CPO) of methane by Pt gauze, targeting a temperature range of 1000−1200 K (727−927 °C) with an inlet CH_4/O_2 ratio of 2.5. Within their targeted temperature range, excessive radicals were reported to be generated and consumed via gas-phase species, such as hydroxyl radicals, which greatly affected the methane conversion in the process. At 750 °C, the gas-phase models of Karakaya and Quiceno already predicted approximately 20 and 25% of overall methane conversion in Figure 1a, respectively. These results indicated that the gas-phase reaction parts were adjusted based on their experimental observations with the presence of catalysts, which degraded the overall accuracy and physical significance of the gas-phase models. Indeed, because the role of the catalyst surface was studied and reported to be a main contributor to the production and quenching of radicals,[18] those excessive radicals should have been generated and consumed within the surface networks instead. This supports the theory that the development of a heterogeneous mechanism should be based first on an accurate gas-phase reaction model, but not *vice versa*. In the later sections, the simulation results from the Karakaya and Quiceno models are not discussed but are still plotted for reference.

Effect of Residence Time and CH_4/O_2 Ratio. In addition to investigating the influence of temperature on the gas-phase OCM, the effect of various residence times (RTs) was studied from 1000 to 3000 ms (1−3 s). From previous reports in the literature, it was determined that the most suitable residence time for this JSR was 0.5−5 s.[57] In eq 6, the total inlet flow rates are adjusted against the reactor temperature to maintain fixed residence times. The temperature was 980 °C, where the gas-phase process was activated with observable profile differences among the models. Figure 2 shows the concentration profile of each main species, measured and plotted against residence time. The conversion of methane and oxygen,

https://doi.org/10.1021/acsomega.1c05020
ACS Omega 2021, 6, 33757−33768

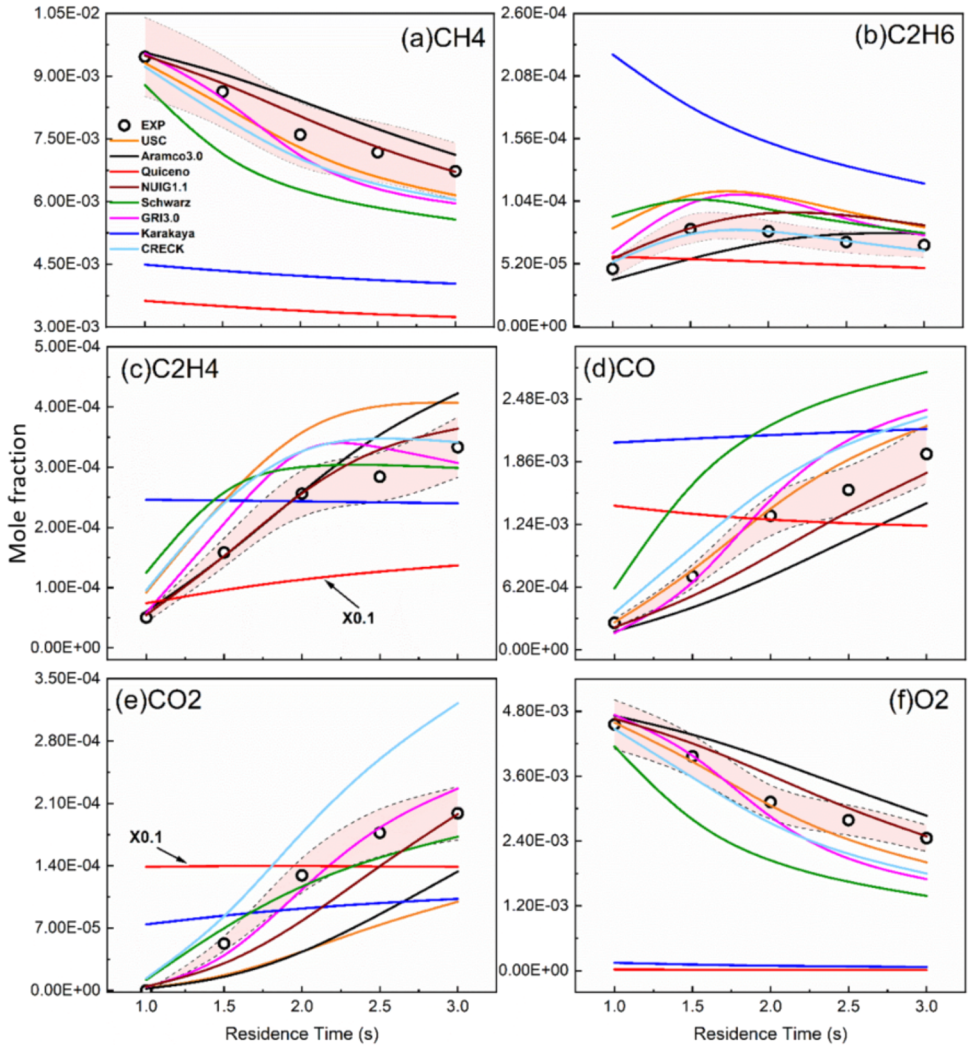

Figure 2. Comparison of mole fraction between experimental (hollow circles) and simulated results (lines with corresponding colors) of (a) CH_4, (b) C_2H_6, (c) C_2H_4, (d) CO, (e) CO_2, and (f) O_2 in the outlet stream against residence time. Operating condition: 1% inlet CH_4, CH_4/O_2 = 2, 101 kPa total pressure, N_2 as balance, and T = 980 °C. Red shadowed regions with dotted lines represent error bars for experimental data.

as well as the production of C_2H_4, CO, and CO_2, increased with residence time; a longer time promoted more reactions within the reactor. However, the concentration of C_2H_6 increased until RT = 1.5 s and then decreased with higher residence times (Figure 2b). This shows that C_2H_6, as the primary product, was formulated mainly at low RTs and then further reacted to other species. In comparison with simulation results against the measured data in Figure 2a,f, USC Mech II, GRI-Mech 3.0, CRECK, NUIGMech1.1, and AramcoMech3.0 successfully captured the trend of reactant consumption and accurately predicted the concentration profiles within a tolerated degree. The Schwarz model once again overestimated the reactant consumption profile. For product formation, the simulation trends of these models generally agreed with the experimental results. USC Mech II, CRECK, GRI-Mech 3.0, and the Schwarz model captured the local concentration maxima of C_2H_6 at RT = 1.5 s. Like the trends of the temperature effect, AramcoMech3.0 showed delayed responses against residence time for the profiles including C_2H_6, C_2H_4, and CO_2. USC Mech II, GRI-Mech 3.0, and NUIGMech1.1 showed good agreement for CO production in Figure 2d, whereas the Schwarz model overestimated CO production. On the other hand, USC Mech II and AramcoMech3.0 underestimated CO_2 production, and CRECK overestimated it, while NUIGMech1.1 and GRI-Mech 3.0 predicted it well within the tolerated range.

Furthermore, the CH_4/O_2 ratio was an important factor for consideration in the OCM process, apparently affecting the overall methane conversion as well as the selectivity of targeted species. In this study, the CH_4/O_2 ratio effect was investigated by varying the inlet oxygen concentrations at a constant methane concentration under the same residence time. The concentration of the main measured products is shown in Figure 3 and compared with simulated concentrations with selected models. From the experimental results, the reactants were barely consumed at high CH_4/O_2 ratios (low oxygen inlet concentrations), where sharp reductions in the formation of all products were observed at CH_4/O_2 ratios higher than 3.5. The typical OCM process with catalysts often operated under high CH_4/O_2 ratios for higher C_2 selectivity, indicating the necessity for the development of a surface reaction mechanism based on accurate gas-phase models. In the comparison of experimental and simulation results in Figure 3, USC Mech II, CRECK, GRI-Mech 3.0, AramcoMech3.0, NUIGMech1.1 and the Schwarz model all captured the trend of the sharp formation reduction at the CH_4/O_2 ratio of 3.5, but the

https://doi.org/10.1021/acsomega.1c05020
ACS Omega 2021, 6, 33757−33768

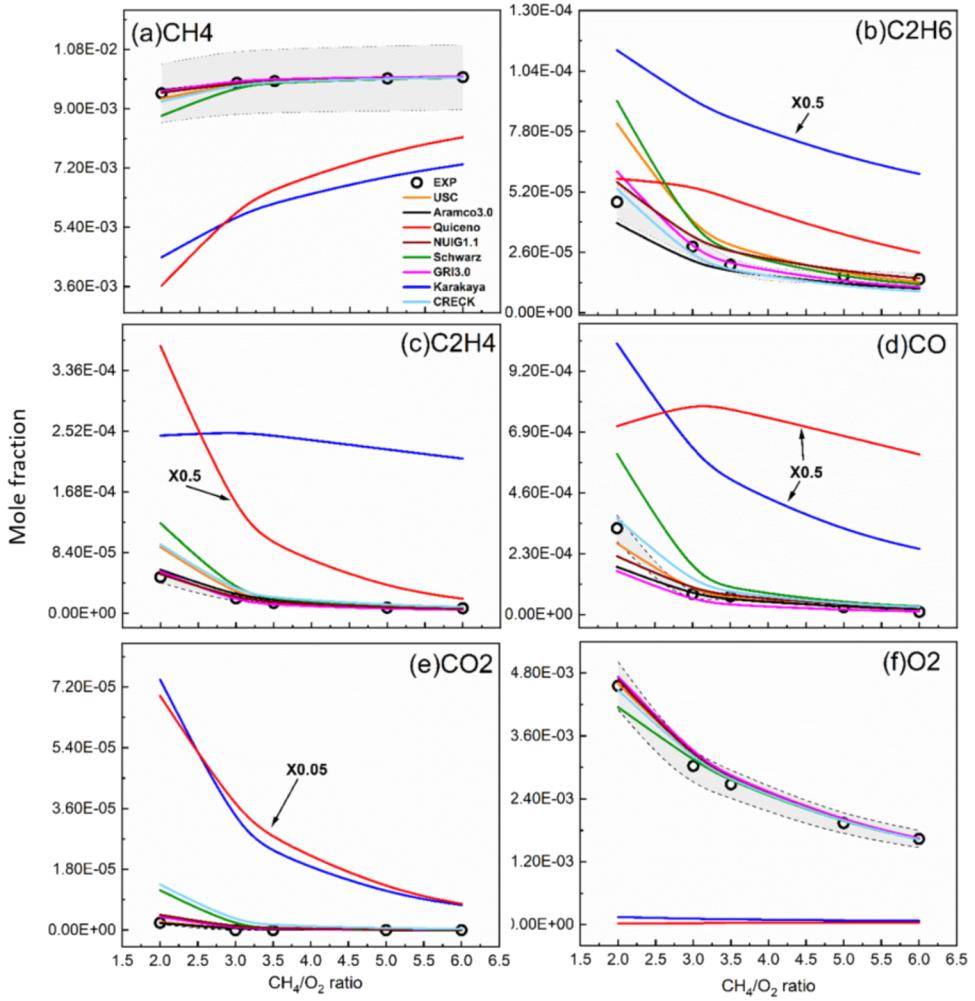

Figure 3. Comparison of mole fraction between experimental (hollow circles) and simulated results (lines with corresponding colors) of (a) CH_4, (b) C_2H_6, (c) C_2H_4, (d) CO, (e) CO_2, and (f) O_2 in the outlet stream against the CH_4/O_2 ratio. Operating condition: 1% inlet CH_4, 101 kPa total pressure, N_2 as balance, RT = 1000 ms, and T = 980 °C. Gray shadowed regions with dotted lines represent error bars for experimental data.

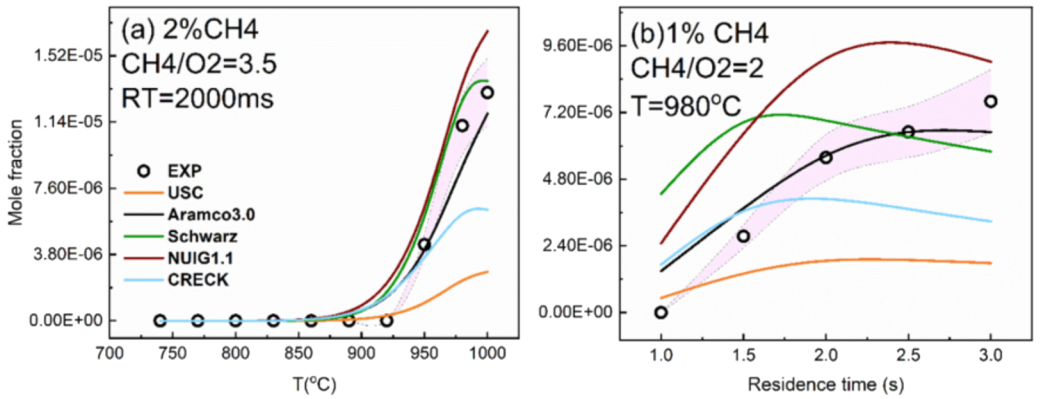

Figure 4. Comparison of mole fraction between experimental (hollow circles) and simulated results (lines with corresponding colors) of C_3H_6 in the outlet stream against (a) temperature and (b) CH_4/O_2 ratio. Operating conditions are shown in each graph, with 101 kPa total pressure and N_2 as balance. Purple shadowed regions with dotted lines represent error bars for experimental data.

reactant consumption and product formation were once again overestimated in the Schwarz model.

Concentration of C_3H_6. Unlike other catalytic processes of methane such as CPO or total oxidation of methane, OCM converts methane into higher hydrocarbons, including C_2, C_3, and even C_4, under fuel-rich operating conditions. Even though they are considered minority species compared to C_2 products,[30,35] higher hydrocarbons such as C_3H_8 and C_3H_6 should be included for a comprehensive OCM kinetic model. In this study, minor C_3H_6 was experimentally detected, and its concentration profile is plotted against temperature and residence time in Figure 4. Similar trends were observed in

https://doi.org/10.1021/acsomega.1c05020
ACS Omega 2021, 6, 33757−33768

other products: The formation of C_3H_6 increased with temperature as well as residence time. In comparison with the experimental results, USC Mech II and CRECK underestimated the concentration profile of C_3H_6 against both temperature and residence time. The description from AramcoMech3.0 agreed well with the experimental data, whereas NUIGMech1.1 captured the trends with slight overestimation. On the other hand, C_3H_6 was not included in the mechanism for GRI-Mech 3.0.

Parity diagrams are plotted in Figure 5 to show the overall comparison of simulated results from different models against

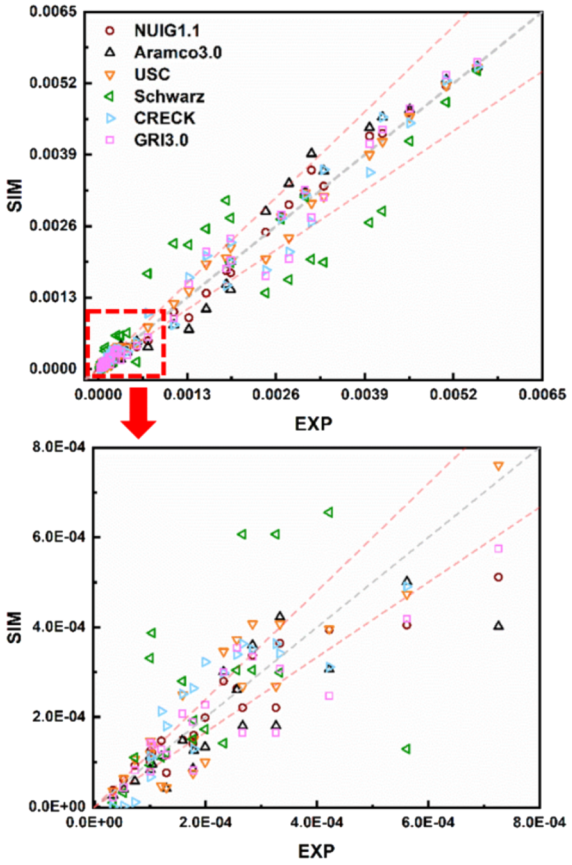

Figure 5. Parity diagrams for main outlet species (O_2, C_2H_6, C_2H_4, CO, and CO_2) of different models against experimental results. Simulation results are calculated by the models, each with a corresponding color. Operating conditions are reported in Table 2. The area between red dashed lines is within the 20% error range of experimental data.

the experimental data under various operating conditions in Table 2. From the comparison, most of the simulated results fit well with the experimental data, except for the Schwarz model for which more outliers could be observed. Other than directly "eyeballing" the analysis, it is better to perform a more quantitative analysis over different models against experimental data. Therefore, quantities of interest (QoI) and traditional rate of production (ROP) analyses were both performed to provide insights and better compare the differences among the models qualitatively.

QoI and ROP Analyses for the Formation of Hydrocarbon Products. The QoI analysis can qualitatively evaluate the difference of reactant or product species profiles between experiment and simulation, while the ROP analysis could identify the key chemical reactions within the kinetic model. By defining different normalized parameters, QoI could well capture the differences within the trend of targeted species profiles, e.g., temperatures and mole fractions at maximum species production or consumption. Also, instead of only targeting a specific reactor temperature for ROP analysis, QoI can evaluate the models across broad temperature ranges. Therefore, both QoI and ROP were implemented, with their own advantages, to complement each other and more thoroughly compare different models in this study.

The parameters for the QoI approach are listed in Table 3, where temperatures and mole fractions are selected based on

Table 3. Definitions of QoI Parameters

QoI parameter	definition
T_1 (in K)	temperature at 1% consumption of reactant minimum or production of species maximum
T_{50} (in K)	temperature at 50% consumption of reactant minimum or production of species maximum
T_m (in K)	temperature at consumption of reactant minimum or production of species maximum
M_{MF}	the mole fraction at consumption of reactant minimum or production of species maximum
$MS = 1 - \frac{T_1^N}{T_1^E}$	normalized temperature differences at 1% consumption of reactant minimum or production of species maximum
$MP = 1 - \frac{T_m^N}{T_m^E}$	normalized temperature differences at consumption of reactant minimum or production of species maximum
$R50 = 1 - \frac{(T_{50} - T_1)^N}{(T_{50} - T_1)^E}$	normalized temperature slope differences at 50% consumption of reactant minimum or production of species maximum
$MMF = 1 - \frac{M_{MF}^N}{M_{MF}^E}$	normalized mole fraction differences at consumption of reactant minimum or production of species maximum

targeted species profiles. Similar to previous studies, several normalized parameters were determined to describe the difference between experimental and simulation results.[78,79] MS was considered as the temperature difference at the starting point of production or consumption of each species. The starting point indicates that the initiation reactions occurred to consume reactants and to produce targeted species. The larger absolute values for MS indicate the larger temperature gaps between experiment and simulation at the starting point. To capture the species being produced or consumed, the parameter *R*50 was introduced to describe the difference in temperature slope at 50% consumption of reactant minimum or production of species maximum. Positive values of *R*50 correspond to the higher production or consumption rates of certain species in simulation than measured in experiment, and *vice versa*. When the targeted species achieve their maximum or minimum, MP and MMF represent the differences in temperature and mole fraction at maximum production or consumption, respectively. Similar to the trends of other parameters, positive values of MP or MMF show the lower maximum temperatures or mole fractions from simulation, and *vice versa*.

Therefore, Figure 7 shows results of QoI parameters for the key species CH_4, C_2H_6, C_2H_4, CO, CO_2, and C_3H_6. For parameters MS and MP, most of values are close to zero for all the models, which indicates that all the models successfully captured the starting point and maximum point over the targeted temperature range. Within this temperature range, the initiation reactions of selected species are well described by all

https://doi.org/10.1021/acsomega.1c05020
ACS Omega 2021, 6, 33757−33768

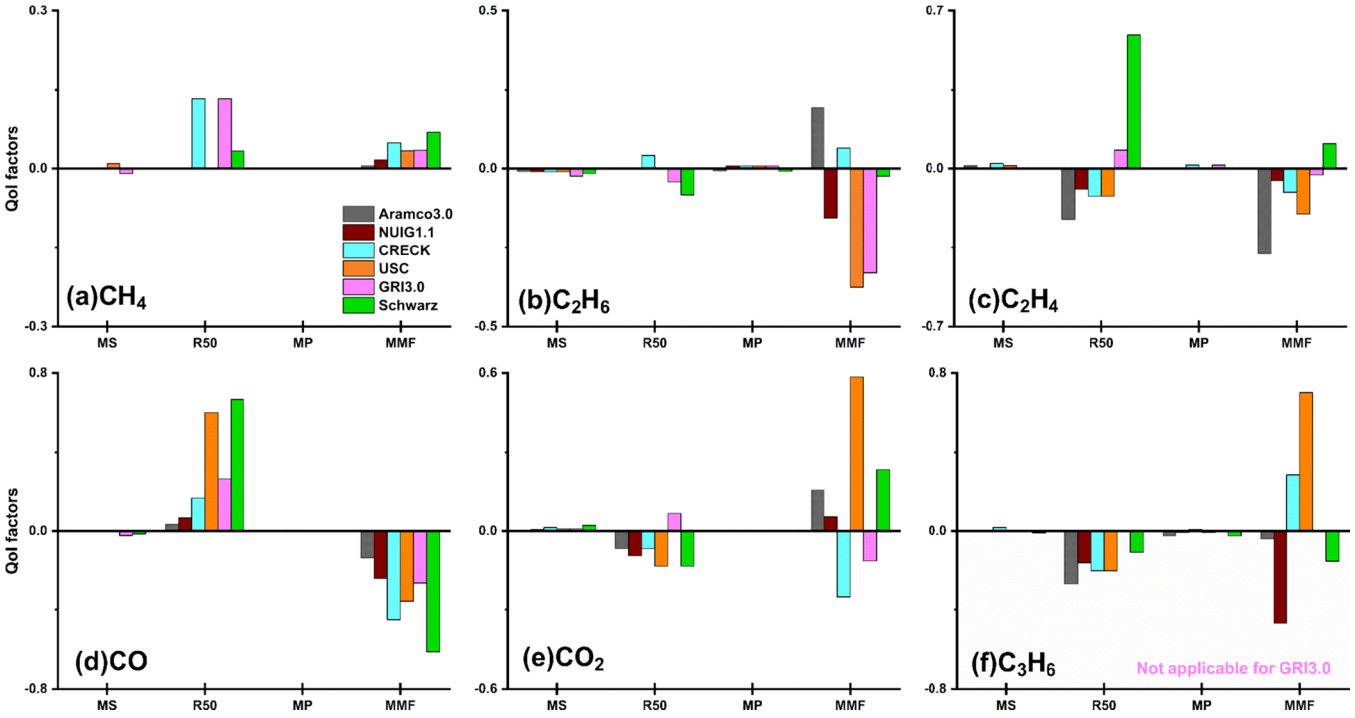

Figure 6. QoI parameter comparison for CH_4, C_2H_6, C_2H_4, CO, CO_2, and C_3H_6 among different models. Operating condition: 5% inlet CH_4, 101 kPa total pressure, N_2 as balance, RT = 2000 ms, and T_{max} = 1000 °C.

models. On the other hand, due to the fuel-rich nature of operating conditions, some species could not reach their maximum at the highest operating temperature such as CO_x, which led to zero values for MP. Indeed, C_2H_6, C_2H_4, and C_3H_6 reached the maximum from experimental results within the temperature range and MP values for those species are also nearly zero, which means that the maximum point temperatures are also well predicted.

For the production and consumption rates represented by *R*50, all models showed good predictions for C_2H_6. The CRECK model and GRI-Mech 3.0 overestimated the consumption rate of methane in Figure 6a. The Schwarz model greatly overestimated the production rate of C_2H_4 and CO and underestimated the production rate of C_2H_6, which might suggest the faster reaction rates of dehydrogenation reactions from C_2H_6 to C_2H_4 to a further oxidation process in the model. USC Mech II also greatly overestimated the CO production rate. On the other hand, for the maximum or minimum mole fractions of each species MMF, the minimum mole fractions of methane were well predicted by all the models. The maximum mole fractions of C_2H_6 were overpredicted by NUIGMech1.1, USC Mech II, and GRI-Mech 3.0 and underpredicted by AramcoMech3.0, while the maximum mole fractions of C_2H_4 were overestimated by AramcoMech3.0 and USC Mech II. For CO, all the models overestimated the maximum mole fraction. Because of the fuel-rich operating conditions, the parameters of CH_4, C_2H_6, C_2H_4, and CO are primarily considered for the best model selection since they are formed or consumed in larger quantities than other species. By considering the primary parameters from QoI analysis, CRECK, NUIGMech1.1, and AramcoMech3.0 are among the models that fit the best against experimental data. By further comparing the absolute values of these parameters, NUIGMech1.1 is selected as the most comprehensively validated for the OCM gas-phase mechanism. Due to the large data set (species and reactions), NUIGMech1.1 should be further reduced to improve the simulation premise, on the premises that the reduced model should keep the overall accuracy and physical significance.

To investigate the key reaction pathways for reactant consumption and product formation, a rate of production (ROP) analysis was performed with hydrocarbon products, as shown in Figure 7. This overall reaction pathway is similar to

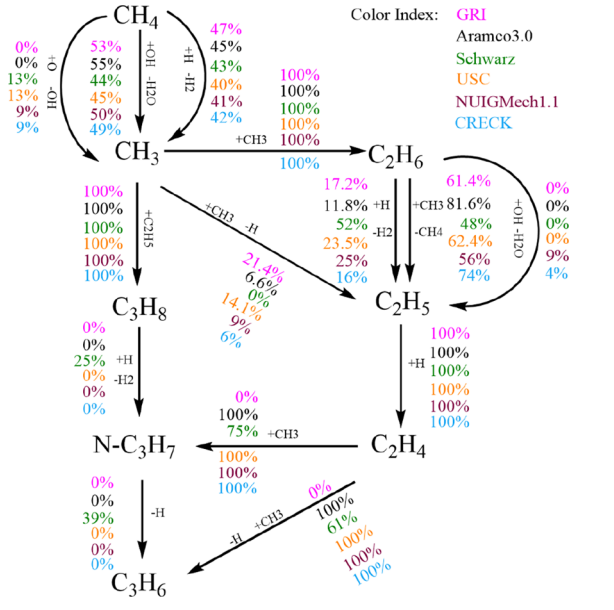

Figure 7. Main reaction pathways for selected gas-phase models on targeted hydrocarbons at 980 °C. Consumption or production percentages shown with corresponding colors. Operating condition: 2% inlet CH_4, CH_4/O_2 = 3.5, 101 kPa total pressure, N_2 as balance, and RT = 2000 ms at the steady state.

https://doi.org/10.1021/acsomega.1c05020
ACS Omega 2021, 6, 33757−33768

Scheme 1. Schematic of the Experimental Setup in This Study

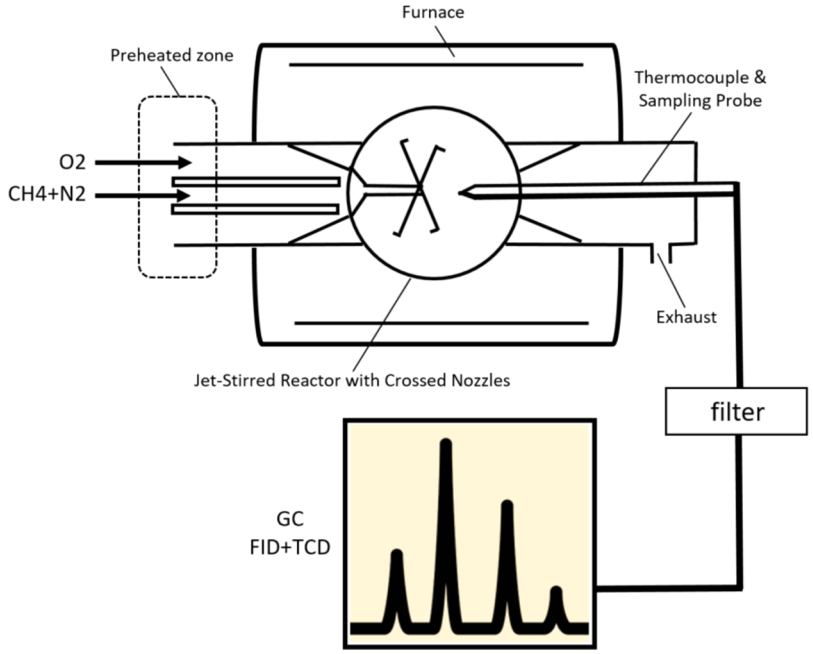

the one previously reported from isotopic studies over gas-phase radicals.[17] All simulations were performed under identical operating conditions. Some common features were observed among the models (Figure 7): The formation of the methyl radical CH_3 was essential for any methane conversion in which all the methane was converted to CH_3 first via different paths of dehydrogenation, ethane was formulated from the recombination of the methyl radicals ($CH_3 + CH_3 = C_2H_6$), ethylene was also generated via the dehydrogenation of ethyl radicals ($C_2H_5 = C_2H_4 + H$), and propane was produced from the recombination between methyl and ethyl radicals ($C_2H_5 + CH_3 = C_3H_8$). However, different pathways were also observed among the models, which could result in different product concentration profiles. GRI-Mech 3.0 did not include C_3 reaction pathways, except for C_3H_8. The Schwarz model highlighted dehydrogenation chain reactions from C_3H_8 to N-C_3H_7 and from N-C_3H_7 to C_3H_6, whereas USC Mech II, NUIGMech1.1, CRECK, and AramcoMech3.0 clarified that $C_2H_4 + CH_3$ contributed 100% to the source of N-C_3H_7 and C_3H_6. On the other hand, the pathways for the ethyl radical C_2H_5, an important intermediate, were different among the models. In Figure 7, C_2H_5 was generated from either hydrogen abstraction from C_2H_6 by H or CH_3 radicals or via CH_3 recombination with simultaneous hydrogen elimination. In all the models, the major source of C_2H_6 is via methyl radical recombination.

CONCLUSIONS

This study experimentally conducted a gas-phase study under OCM conditions in a jet-stirred reactor (0-D reactor); simulations were also performed with nine selected gas-phase kinetic models. Various operating parameters, including temperatures, residence times, and inlet CH_4/O_2 ratios, were investigated for this comprehensive study. Comparing experimental and simulation results, AramcoMech3.0, the CRECK model, NUIGMech1.1, GRI-Mech 3.0, the Schwarz model, and USC Mech II successfully captured the trends under different operating conditions for OCM. In contrast, the Sun model, Karakaya model, and Quiceno model, the models adopted from the catalytic process, barely followed the experimental trends, indicating that their gas-phase kinetics were modified based on observations from a coupled heterogeneous network. By performing QoI analysis, all the models were evaluated against experimental results and NUIGMech1.1 was found to be the best model to describe OCM gas-phase kinetics, including the formation of C_3 species. For an accurate OCM model, a heterogeneous mechanism should be developed based on an accurate gas-phase reaction model, and NUIGMech1.1 is recommended as the gas-phase model for future heterogeneous model construction.

EXPERIMENTAL AND SIMULATION METHODS

This study employed a jet-stirred reactor (JSR) to investigate OCM gas-phase kinetics, similar to previous works by this group.[80,81] Detailed descriptions of JSR are available in the published literature.[82,83] The schematic of the experimental setup is shown in Scheme 1. Briefly, a spherical reactor with a total volume of 76 cm^3 is made of fused silica to minimize wall-catalyzed reactions between the wall and the intermediate species. Four crossed nozzles within the reactor (I.D. of 0.3 mm) create stirring jet flows and ideal mixing of the inlet streams. From a previous study,[57] a JSR with crossed nozzles with inner diameters greater than 0.2 mm (I.D. > 0.2 mm) allow for better mixing. A suitable range of residence time (0.5−5 s) was carefully selected, corresponding to the reactor volume with crossed nozzles. Ideal mixing assumptions are valid under these geometrical and operation conditions. Nitrogen was selected as the carrier gas and diluent, cofeeding with methane and oxygen as the inlet stream. The inlet methane and oxygen were preheated and introduced separately through different channels so that no reaction would occur before the nozzle injection. The JSR was heated by a furnace to the target temperature, and a K-type thermocouple was located in a thin silica tube to avoid catalytic effects and placed inside the reactor to monitor the reaction temperature. To maintain fixed residence times, the gas flow rates were adjusted based on

https://doi.org/10.1021/acsomega.1c05020
ACS Omega 2021, 6, 33757−33768

the measured reactor temperature and controlled by MKS mass flow controllers. The temperature homogeneity within the reactor was tested with a pure nitrogen flow and showed good uniformity (<3 °C/cm). The outlet stream was then sampled by a sonic-throat gas sampling probe connected to a mechanical pump to create a pressure drop that prevented further reactions of the outlets. The sampled gas was analyzed using an Agilent refinery gas analyzer (RGA). The carbon balance (average of 95%) under each operating condition is calculated and reported in the Supporting Information.

Simulations of the JSR were performed using the perfectly-stirred reactor module (PSR) in CHEMKIN-PRO.[84] The reactor was modeled as zero-dimensional (0-D), with an end time of 50 s of the transient solver to achieve steady-state criteria. Because of the significant temperature homogeneity and negligible temperature profile along the reactor, the reactor model was set as isothermal. The input inlet compositions, temperatures, and calculated residence times in simulation corresponded to the operating conditions in the experiment in Table 2. The residence time τ is calculated in eq 7, where ρ is the mass density, which is related to the pressure and temperature, V is the volume of reactor, and $\dot{m}$ is the mass flow rate of the inlet stream.

$$\tau = \rho V / \dot{m} \tag{7}$$

■ ASSOCIATED CONTENT

Supporting Information

The Supporting Information is available free of charge at https://pubs.acs.org/doi/10.1021/acsomega.1c05020.

Details of carbon balance calculations under each reported operating condition (PDF)

■ AUTHOR INFORMATION

Corresponding Authors

Haoyi Wang − *Clean Combustion Research Center (CCRC), Physical Sciences and Engineering Division and KAUST Catalysis Center (KCC), Physical Sciences and Engineering Division, King Abdullah University of Science and Technology (KAUST), Thuwal 23955-6900, Saudi Arabia;* orcid.org/0000-0002-6865-0646; Email: haoyi.wang@kaust.edu.sa

S. Mani Sarathy − *Clean Combustion Research Center (CCRC), Physical Sciences and Engineering Division and KAUST Catalysis Center (KCC), Physical Sciences and Engineering Division, King Abdullah University of Science and Technology (KAUST), Thuwal 23955-6900, Saudi Arabia;* orcid.org/0000-0002-3975-6206; Email: mani.sarathy@kaust.edu.sa

Authors

Can Shao − *Clean Combustion Research Center (CCRC), Physical Sciences and Engineering Division, King Abdullah University of Science and Technology (KAUST), Thuwal 23955-6900, Saudi Arabia*

Jorge Gascon − *KAUST Catalysis Center (KCC), Physical Sciences and Engineering Division, King Abdullah University of Science and Technology (KAUST), Thuwal 23955-6900, Saudi Arabia;* orcid.org/0000-0001-7558-7123

Kazuhiro Takanabe − *Department of Chemical System Engineering, School of Engineering, The University of Tokyo, Bunkyo-ku, Tokyo 113-8656, Japan; Japan Science and Technology Agency (JST), PRESTO, Kawaguchi, Saitama 332-0012, Japan;* orcid.org/0000-0001-5374-9451

Complete contact information is available at: https://pubs.acs.org/10.1021/acsomega.1c05020

Notes

The authors declare no competing financial interest.

■ ACKNOWLEDGMENTS

The work at King Abdullah University of Science and Technology (KAUST) is supported by the Office of Sponsored Research with funding from the Clean Combustion Research Center and KAUST Catalysis Center.

■ REFERENCES

(1) Keller, G. E.; Bhasin, M. M. Synthesis of ethylene via oxidative coupling of methane: I Determination of active catalysts. *J. Catal.* **1982**, *73*, 9−19.

(2) Wu, X. Y.; Tang, Z.; Zhao, X.; Luo, X.; Pennycook, S. J.; Wang, S. L. Visible-light driven room-temperature coupling of methane to ethane by atomically dispersed Au on WO3. *J. Energy Chem.* **2021**, *61*, 195−202.

(3) Sato, A.; Ogo, S.; Kamata, K.; Takeno, Y.; Yabe, T.; Yamamoto, T.; Matsumura, S.; Hara, M.; Sekine, Y. Ambient-temperature oxidative coupling of methane in an electric field by a cerium phosphate nanorod catalyst. *Chem. Commun.* **2019**, *55*, 4019−4022.

(4) Schammel, W. P.; Wolfenbarger, J.; Ajinkya, M.; McCarty, J.; Cizeron, J. M.; Weinberger, S.; Edwards, J. D.; Sheridan, D.; Scher, E. C.; McCormick, J. Oxidative coupling of methane systems and methods. U.S. Patent No. 9,556,086 B2, 2017.

(5) Cizeron, J.; Radaelli, G.; Lakhapatri, S.; Freer, E.; Hong, J. K.; McCormick, J.; Sheridan, D.; Reid, C.; Pellizzari, R.; Weinberger, S. Reactors and systems for oxidative coupling of methane. U.S. Patent No. 10,047,020, 2018.

(6) Lunsford, J. H. Catalytic conversion of methane to more useful chemicals and fuels: a challenge for the 21st century. *Catal. Today* **2000**, *63*, 165−174.

(7) Pak, S.; Qiu, P.; Lunsford, J. H. Elementary reactions in the oxidative coupling of methane over Mn/Na2WO4/SiO2 and Mn/Na2WO4/MgO catalysts. *J. Catal.* **1998**, *179*, 222−230.

(8) Takanabe, K.; Iglesia, E. Mechanistic Aspects and Reaction Pathways for Oxidative Coupling of Methane on Mn/Na2WO4/SiO2 Catalysts. *J. Phys. Chem. C* **2009**, *113*, 10131−10145.

(9) Karakaya, C.; Kee, R. J. Progress in the direct catalytic conversion of methane to fuels and chemicals. *Prog. Energy Combust. Sci.* **2016**, *55*, 60−97.

(10) Lomonosov, V. I.; Sinev, M. Y. Oxidative coupling of methane: Mechanism and kinetics. *Kinet. Catal.* **2016**, *57*, 647−676.

(11) Kiani, D.; Sourav, S.; Baltrusaitis, J.; Wachs, I. E. Oxidative Coupling of Methane (OCM) by SiO2-Supported Tungsten Oxide Catalysts Promoted with Mn and Na. *ACS Catal.* **2019**, *9*, 5912−5928.

(12) Takanabe, K.; Iglesia, E. Rate and selectivity enhancements mediated by OH radicals in the oxidative coupling of methane catalyzed by Mn/Na2WO4/SiO2. *Angew. Chem., Int. Ed.* **2008**, *47*, 7689−7693.

(13) Al-Zahrani, S. M. S.; Lobban, L. L. Effects of Steam and Liquid Water Treatment on the Oxidative Coupling of Methane over a Li/MgO Catalyst. *Ind. Eng. Chem. Res.* **1995**, *34*, 1060−1073.

(14) Takanabe, K.; Khan, A. M.; Tang, Y.; Nguyen, L.; Ziani, A.; Jacobs, B. W.; Elbaz, A. M.; Sarathy, S. M.; Tao, F. F. Integrated In Situ Characterization of a Molten Salt Catalyst Surface: Evidence of Sodium Peroxide and Hydroxyl Radical Formation. *Angew. Chem., Int. Ed.* **2017**, *56*, 10403−10407.

(15) Li, D.; Baslyman, W. S.; Sarathy, S. M.; Takanabe, K. Impact of OH Radical Generator Involvement in the Gas-Phase Radical

Reaction Network on the Oxidative Coupling of Methane—A Simulation Study. *Energy Technol.* **2020**, *8*, 1900563.
(16) Shi, C.; Hatano, M.; Lunsford, J. H. A Kinetic-Model for the Oxidative Coupling of Methane over Li+/Mgo Catalysts. *Catal. Today* **1992**, *13*, 191−199.
(17) Mims, C. A.; Mauti, R.; Dean, A. M.; Rose, K. D. Radical Chemistry in Methane Oxidative Coupling - Tracing of Ethylene Secondary Reactions with Computer-Models and Isotopes. *J. Phys Chem.*. **1994**, *98*, 13357−13372.
(18) Couwenberg, P. M.; Chen, Q.; Marin, G. B. Kinetics of a gas-phase chain reaction catalyzed by a solid: The oxidative coupling of methane over Li/MgO-based catalysts. *Ind. Eng. Chem. Res.* **1996**, *35*, 3999−4011.
(19) Chen, Q.; Couwenberg, P. M.; Marin, G. B. Effect of Pressure on the Oxidative Coupling of Methane in the Absence of Catalyst. *AIChE J.* **1994**, *40*, 521−535.
(20) Alexiadis, V. I.; Chaar, M.; van Veen, A.; Muhler, M.; Thybaut, J. W.; Marin, G. B. Quantitative screening of an extended oxidative coupling of methane catalyst library. *Appl. Catal., B* **2016**, *199*, 252−259.
(21) Alexiadis, V. I.; Thybaut, J. W.; Kechagiopoulos, P. N.; Chaar, M.; Van Veen, A. C.; Muhler, M.; Marin, G. B. Oxidative coupling of methane: catalytic behaviour assessment via comprehensive micro-kinetic modelling. *Appl. Catal., B* **2014**, *150-151*, 496−505.
(22) Kechagiopoulos, P. N.; Thybaut, J. W.; Marin, G. B. Oxidative Coupling of Methane: A Microkinetic Model Accounting for Intraparticle Surface-Intermediates Concentration Profiles. *Ind. Eng. Chem. Res.* **2013**, *53*, 1825−1840.
(23) Pirro, L.; Mendes, P. S. F.; Paret, S.; Vandegehuchte, B. D.; Marin, G. B.; Thybaut, J. W. Descriptor−property relationships in heterogeneous catalysis: exploiting synergies between statistics and fundamental kinetic modelling. *Catal. Sci. Technol.* **2019**, *9*, 3109−3125.
(24) Pirro, L.; Mendes, P. S. F.; Vandegehuchte, B. D.; Marin, G. B.; Thybaut, J. W. Catalyst screening for the oxidative coupling of methane: from isothermal to adiabatic operation via microkinetic simulations. *React. Chem. Eng.* **2020**, *5*, 584−596.
(25) Pirro, L.; Obradović, A.; Vandegehuchte, B. D.; Marin, G. B.; Thybaut, J. W. Model-Based Catalyst Selection for the Oxidative Coupling of Methane in an Adiabatic Fixed-Bed Reactor. *Ind. Eng. Chem. Res.* **2018**, *57*, 16295−16307.
(26) Sun, J.; Thybaut, J.; Marin, G. Microkinetics of methane oxidative coupling. *Catal. Today* **2008**, *137*, 90−102.
(27) Thybaut, J. W.; Sun, J.; Olivier, L.; Van Veen, A. C.; Mirodatos, C.; Marin, G. B. Catalyst design based on microkinetic models: Oxidative coupling of methane. *Catal. Today* **2011**, *159*, 29−36.
(28) Vandewalle, L. A.; Lengyel, I.; West, D. H.; Van Geem, K. M.; Marin, G. B. Catalyst ignition and extinction: A microkinetics-based bifurcation study of adiabatic reactors for oxidative coupling of methane. *Chem. Eng. Sci.* **2019**, *199*, 635−651.
(29) Vandewalle, L. A.; Van de Vijver, R.; Van Geem, K. M.; Marin, G. B. The role of mass and heat transfer in the design of novel reactors for oxidative coupling of methane. *Chem. Eng. Sci.* **2019**, *198*, 268−289.
(30) Karakaya, C.; Zhu, H.; Zohour, B.; Senkan, S.; Kee, R. J. Detailed Reaction Mechanisms for the Oxidative Coupling of Methane over La2O3/CeO2 Nanofiber Fabric Catalysts. *ChemCatChem* **2017**, *9*, 4538−4551.
(31) Karakaya, C.; Zhu, H.; Loebick, C.; Weissman, J. G.; Kee, R. J. A detailed reaction mechanism for oxidative coupling of methane over Mn/Na2WO4/SiO2 catalyst for non-isothermal conditions. *Catal. Today* **2018**, *312*, 10−22.
(32) Chen, Q.; Hoebink, J. H. B. J.; Marin, G. B. Kinetics of the Oxidative Coupling of Methane at Atmospheric-Pressure in the Absence of Catalyst. *Ind. Eng. Chem. Res.* **1991**, *30*, 2088−2097.
(33) Sekine, Y.; Nishimura, T.; Fujimoto, K. Oxidative coupling of methane in the gas phase: Simulation and reaction mechanism. *Energy Fuels* **1998**, *12*, 828−829.
(34) Zanthoff, H.; Baerns, M. Oxidative Coupling of Methane in the Gas-Phase. Kinetic Simulation and Experimental-Verification. *Ind. Eng. Chem. Res.* **1990**, *29*, 2−10.
(35) Luo, L.; You, R.; Liu, Y.; Yang, J.; Zhu, Y.; Wen, W.; Pan, Y.; Qi, F.; Huang, W. Gas-Phase Reaction Network of Li/MgO-Catalyzed Oxidative Coupling of Methane and Oxidative Dehydrogenation of Ethane. *ACS Catal.* **2019**, *9*, 2514−2520.
(36) Ishioka, S.; Miyazato, I.; Takahashi, L.; Nguyen, T. N.; Taniike, T.; Takahashi, K. Unveiling gas-phase oxidative coupling of methane via data analysis. *J. Comput. Chem.* **2021**, *42*, 1447−1451.
(37) Takanabe, K. Catalytic Conversion of Methane: Carbon Dioxide Reforming and Oxidative Coupling. *J. Jpn. Pet. Inst.* **2012**, *55*, 1−12.
(38) Liang, Y.; Li, Z.; Nourdine, M.; Shahid, S.; Takanabe, K. Methane Coupling Reaction in an Oxy-Steam Stream through an OH Radical Pathway by using Supported Alkali Metal Catalysts. *ChemCatChem* **2014**, *6*, 1245−1251.
(39) Fleischer, V.; Steuer, R.; Parishan, S.; Schomäcker, R. Investigation of the surface reaction network of the oxidative coupling of methane over Na2WO4/Mn/SiO2 catalyst by temperature programmed and dynamic experiments. *J. Catal.* **2016**, *341*, 91−103.
(40) Kalenik, Z.; Wolf, E. E. Transient And Isotopic Studies Of The Oxygen Transport And Exchange During Oxidative Coupling Of Methane On Sr Promoted La2o3. *Catal. Lett.* **1991**, *9*, 441−449.
(41) Lacombe, S.; Zanthoff, H.; Mirodatos, C. Oxidative Coupling of Methane over Lanthana Catalysts. 2. A Mechanistic Study Using Isotope Transient Kinetics. *J. Catal.* **1995**, *155*, 106−116.
(42) Shi, C.; Xu, M.; Rosynek, M. P.; Lunsford, J. H. Origin of kinetic isotope effects during the oxidative coupling of methane over a lithium(1+)/magnesia catalyst. *J. Phys. Chem.* **1993**, *97*, 216−222.
(43) Ishikawa, A.; Tateyama, Y. A First-Principles Microkinetics for Homogeneous−Heterogeneous Reactions: Application to Oxidative Coupling of Methane Catalyzed by Magnesium Oxide. *ACS Catal.* **2021**, *11*, 2691−2700.
(44) Wang, S.; Cong, L.; Zhao, C.; Li, Y.; Pang, Y.; Zhao, Y.; Li, S.; Sun, Y. First principles studies of CO2 and O2 chemisorption on La2O3 surfaces. *Phys. Chem. Chem. Phys.* **2017**, *19*, 26799−26811.
(45) Lei, Y.; Chu, C.; Li, S.; Sun, Y. Methane Activations by Lanthanum Oxide Clusters. *J. Phys. Chem. C* **2014**, *118*, 7932−7945.
(46) Chu, C.; Zhao, Y.; Li, S.; Sun, Y. Role of Peroxides on La2O3 Catalysts in Oxidative Coupling of Methane. *J. Phys. Chem. C* **2014**, *118*, 27954−27960.
(47) Chu, C.; Zhao, Y.; Li, S.; Sun, Y. Correlation between the acid-base properties of the La2O3 catalyst and its methane reactivity. *Phys. Chem. Chem. Phys.* **2016**, *18*, 16509−16517.
(48) Palmer, M. S.; Neurock, M.; Olken, M. M. Periodic Density Functional Theory Study of Methane Activation over La2O3: Activity of O2-, O-, O22-, Oxygen Point Defect, and Sr2+-Doped Surface Sites. *J. Am. Chem. Soc.* **2002**, *124*, 8452−8461.
(49) Studt, F.; Sharafutdinov, I.; Abild-Pedersen, F.; Elkjær, C. F.; Hummelshøj, J. S.; Dahl, S.; Chorkendorff, I.; Nørskøv, J. K. Discovery of a Ni-Ga catalyst for carbon dioxide reduction to methanol. *Nat. Chem.* **2014**, *6*, 320−324.
(50) Schwach, P.; Pan, X.; Bao, X. Direct Conversion of Methane to Value-Added Chemicals over Heterogeneous Catalysts: Challenges and Prospects. *Chem. Rev.* **2017**, *117*, 8497−8520.
(51) Cong, L.; Zhao, Y.; Li, S.; Sun, Y. Sr-doping effects on La 2 O 3 catalyst for oxidative coupling of methane. *Chin. J. Catal.* **2017**, *38*, 899−907.
(52) Kumar, G.; Lau, S. L. J.; Krcha, M. D.; Janik, M. J. Correlation of Methane Activation and Oxide Catalyst Reducibility and Its Implications for Oxidative Coupling. *ACS Catal.* **2016**, *6*, 1812−1821.
(53) Jiang, T.; Song, J.; Huo, M.; Yang, N.; Liu, J.; Zhang, J.; Sun, Y.; Zhu, Y. La2O3 catalysts with diverse spatial dimensionality for oxidative coupling of methane to produce ethylene and ethane. *RSC Adv.* **2016**, *6*, 34872−34876.
(54) Hou, Y.-H.; Han, W.-C.; Xia, W.-S.; Wan, H.-L. Structure Sensitivity of La2O2CO3 Catalysts in the Oxidative Coupling of Methane. *ACS Catal.* **2015**, *5*, 1663−1674.

https://doi.org/10.1021/acsomega.1c05020
ACS Omega 2021, 6, 33757−33768

(55) Schwarz, H.; Geske, M.; Franklin Goldsmith, C.; Schlögl, R.; Horn, R. Fuel-rich methane oxidation in a high-pressure flow reactor studied by optical-fiber laser-induced fluorescence, multi-species sampling profile measurements and detailed kinetic simulations. *Combust. Flame* **2014**, *161*, 1688−1700.
(56) Monge, F.; Aranda, V.; Millera, A.; Bilbao, R.; Alzueta, M. U. Tubular Flow Reactors. In *Cleaner Combustion: Developing Detailed Chemical Kinetic Models;* Battin-Leclerc, F.; Simmie, J. M.; Blurock, E. Eds. Springer London: London, 2013; pp. 211−230.
(57) Ayass, W. W.; Nasir, E. F.; Farooq, A.; Sarathy, S. M. Mixing-structure relationship in jet-stirred reactors. *Chem. Eng. Res. Des.* **2016**, *111*, 461−464.
(58) Herbinet, O.; Dayma, G. Jet-Stirred Reactors. In *Cleaner Combustion: Developing Detailed Chemical Kinetic Models;* Battin-Leclerc, F.; Simmie, J. M.; Blurock, E. Eds. Springer London: London, 2013; pp. 183−210.
(59) Zhou, C.-W.; Li, Y.; Burke, U.; Banyon, C.; Somers, K. P.; Ding, S.; Khan, S.; Hargis, J. W.; Sikes, T.; Mathieu, O.; Petersen, E. L.; AlAbbad, M.; Farooq, A.; Pan, Y.; Zhang, Y.; Huang, Z.; Lopez, J.; Loparo, Z.; Vasu, S. S.; Curran, H. J. An experimental and chemical kinetic modeling study of 1,3-butadiene combustion: Ignition delay time and laminar flame speed measurements. *Combust. Flame* **2018**, *197*, 423−438.
(60) Li, Y.; Zhou, C.-W.; Somers, K. P.; Zhang, K.; Curran, H. J. The oxidation of 2-butene: A high pressure ignition delay, kinetic modeling study and reactivity comparison with isobutene and 1-butene. *Proc. Combust. Inst.* **2017**, *36*, 403−411.
(61) Bagheri, G.; Ranzi, E.; Pelucchi, M.; Parente, A.; Frassoldati, A.; Faravelli, T. Comprehensive kinetic study of combustion technologies for low environmental impact: MILD and OXY-fuel combustion of methane. *Combust. Flame* **2020**, *212*, 142−155.
(62) Smith, G. P.; Golden, D. M.; Frenklach, M.; Moriarty, N. W.; Eiteneer, B.; Goldenberg, M.; Bowman, C. T.; Hanson, R. K.; Song, S.; Gardiner, W. C.; V, V. L., Jr.; Qin, Z. http://www.me.berkeley.edu/gri_mech/.
(63) Baigmohammadi, M.; Patel, V.; Martinez, S.; Panigrahy, S.; Ramalingam, A.; Burke, U.; Somers, K. P.; Heufer, K. A.; Pekalski, A.; Curran, H. J. A Comprehensive Experimental and Simulation Study of Ignition Delay Time Characteristics of Single Fuel C1−C2 Hydrocarbons over a Wide Range of Temperatures, Pressures, Equivalence Ratios, and Dilutions. *Energy Fuels* **2020**, *34*, 3755−3771.
(64) Quiceno, R.; Pérez-Ramírez, J.; Warnatz, J.; Deutschmann, O. Modeling the high-temperature catalytic partial oxidation of methane over platinum gauze: Detailed gas-phase and surface chemistries coupled with 3D flow field simulations. *Appl. Catal., A* **2006**, *303*, 166−176.
(65) Wang, H.; You, X.; Joshi, A. V.; Davis, S. G.; Laskin, A.; Egolfopoulos, F.; Law, C. K. *USC Mech Version II. High-Temperature Combustion Reaction Model of H2/CO/C1-C4 Compounds.* http://ignis.usc.edu/USC_Mech_II.htm.
(66) Metcalfe, W. K.; Burke, S. M.; Ahmed, S. S.; Curran, H. J. A Hierarchical and Comparative Kinetic Modeling Study of C1−C2 Hydrocarbon and Oxygenated Fuels. *Int. J. Chem. Kinet.* **2013**, *45*, 638−675.
(67) Burke, S. M.; Burke, U.; Mc Donagh, R.; Mathieu, O.; Osorio, I.; Keesee, C.; Morones, A.; Petersen, E. L.; Wang, W.; DeVerter, T. A.; Oehlschlaeger, M. A.; Rhodes, B.; Hanson, R. K.; Davidson, D. F.; Weber, B. W.; Sung, C.-J.; Santner, J.; Ju, Y.; Haas, F. M.; Dryer, F. L.; Volkov, E. N.; Nilsson, E. J. K.; Konnov, A. A.; Alrefae, M.; Khaled, F.; Farooq, A.; Dirrenberger, P.; Glaude, P.-A.; Battin-Leclerc, F.; Curran, H. J. An experimental and modeling study of propene oxidation. Part 2: Ignition delay time and flame speed measurements. *Combust. Flame* **2015**, *162*, 296−314.
(68) Dooley, S.; Burke, M. P.; Chaos, M.; Stein, Y.; Dryer, F. L.; Zhukov, V. P.; Finch, O.; Simmie, J. M.; Curran, H. J. Methyl formate oxidation: Speciation data, laminar burning velocities, ignition delay times, and a validated chemical kinetic model. *Int. J. Chem. Kinet.* **2010**, *42*, 527−549.
(69) Karbach, V. *Validierung eines detaillierten Reaktionsmechanismus zur Oxidation von Kohlenwasserstoffen bei hohen Temperaturen*; Fakultaet Chemie der Ruprecht-Karls-Universitaet Heidelberg: Heidelberg, Germany. 1997.
(70) Baigmohammadi, M.; Patel, V.; Nagaraja, S.; Ramalingam, A.; Martinez, S.; Panigrahy, S.; Mohamed, A. A. E.-S.; Somers, K. P.; Burke, U.; Heufer, K. A.; Pekalski, A.; Curran, H. J. Comprehensive Experimental and Simulation Study of the Ignition Delay Time Characteristics of Binary Blended Methane, Ethane, and Ethylene over a Wide Range of Temperature, Pressure, Equivalence Ratio, and Dilution. *Energy Fuels* **2020**, *34*, 8808−8823.
(71) Nagaraja, S. S.; Liang, J.; Dong, S.; Panigrahy, S.; Sahu, A.; Kukkadapu, G.; Wagnon, S. W.; Pitz, W. J.; Curran, H. J. A hierarchical single-pulse shock tube pyrolysis study of C2−C6 1-alkenes. *Combust. Flame* **2020**, *219*, 456−466.
(72) El-Sabor Mohamed, A. A.; Panigrahy, S.; Sahu, A. B.; Bourque, G.; Curran, H. J. An experimental and kinetic modeling study of the auto-ignition of natural gas blends containing C1−C7 alkanes. *Proc. Combust. Inst.* **2021**, *38*, 365−373.
(73) Martinez, S.; Baigmohammadi, M.; Patel, V.; Panigrahy, S.; Sahu, A. B.; Nagaraja, S. S.; Ramalingam, A.; Mohamed, A. A. E.-S.; Somers, K. P.; Heufer, K. A.; Pekalski, A.; Curran, H. J. An experimental and kinetic modeling study of the ignition delay characteristics of binary blends of ethane/propane and ethylene/propane in multiple shock tubes and rapid compression machines over a wide range of temperature, pressure, equivalence ratio, and dilution. *Combust. Flame* **2021**, *228*, 401−414.
(74) Davis, S. G.; Law, C. K.; Wang, H. Propene pyrolysis and oxidation kinetics in a flow reactor and laminar flames. *Combust. Flame* **1999**, *119*, 375−399.
(75) Davis, S. G.; Joshi, A. V.; Wang, H.; Egolfopoulos, F. An optimized kinetic model of H2/CO combustion. *Proc. Combust. Inst.* **2005**, *30*, 1283−1292.
(76) Laskin, A.; Wang, H.; Law, C. K. Detailed kinetic modeling of 1,3-butadiene oxidation at high temperatures. *Int. J. Chem. Kinet.* **2000**, *32*, 589−614.
(77) Le Cong, T.; Dagaut, P.; Dayma, G. Oxidation of natural gas, natural gas/syngas mixtures, and effect of burnt gas recirculation: Experimental and detailed kinetic modeling. *J. Eng. Gas Turbines Power.* **2008**, *130*, No. 041502.
(78) Chen, B.; Togbé, C.; Selim, H.; Dagaut, P.; Sarathy, S. M. Quantities of Interest in Jet Stirred Reactor Oxidation of a High-Octane Gasoline. *Energy Fuels* **2017**, *31*, 5543−5553.
(79) Selim, H.; Mohamed, S. Y.; Dawood, A. E.; Sarathy, S. M. Understanding premixed flame chemistry of gasoline fuels by comparing quantities of interest. *Proc. Combust. Inst.* **2017**, *36*, 1203−1211.
(80) Shao, C.; Wang, H.; Atef, N.; Wang, Z.; Chen, B.; Almalki, M.; Zhang, Y.; Cao, C.; Yang, J.; Sarathy, S. M. Polycyclic aromatic hydrocarbons in pyrolysis of gasoline surrogates (n-heptane/iso-octane/toluene). *Proc. Combust. Inst.* **2019**, *37*, 993−1001.
(81) Chen, B.; Wang, Z.; Wang, J.-Y.; Wang, H.; Togbé, C.; Alonso, P. E. A.; Almalki, M.; Mehl, M.; Pitz, W. J.; Wagnon, S. W.; Zhang, K.; Kukkadapu, G.; Dagaut, P.; Mani Sarathy, S. Exploring gasoline oxidation chemistry in jet stirred reactors. *Fuel* **2019**, *236*, 1282−1292.
(82) Dagaut, P.; Cathonnet, M.; J P Rouan, R. F.; A Quilgars, J. C. B.; Gaillard, F.; James, H. A jet-stirred reactor for kinetic studies of homogeneous gas-phase reactions at pressures up to ten atmospheres (≈1 MPa). *J. Phys. E: Sci. Instrum.* **1986**, *19*, 207.
(83) Dagaut, P.; Karsenty, F.; Dayma, G.; Diévart, P.; Hadj-Ali, K.; Mzé-Ahmed, A.; Braun-Unkhoff, M.; Herzler, J.; Kathrotia, T.; Kick, T.; Naumann, C.; Riedel, U.; Thomas, L. Experimental and detailed kinetic model for the oxidation of a Gas to Liquid (GtL) jet fuel. *Combust. Flame* **2014**, *161*, 835−847.
(84) *CHEMKIN-PRO 15112, Reaction Design: San Diego;* 2012.

https://doi.org/10.1021/acsomega.1c05020
ACS Omega 2021, 6, 33757−33768